

Contents lists available at ScienceDirect

Materials Today Advances

journal homepage: www.journals.elsevier.com/materials-today-advances/





Data-driven discovery of novel metal organic frameworks with superior ammonia adsorption capacity

Sanghyun Kim, Joo-Hyoung Lee

School of Materials Science and Engineering, Gwangju Institute of Science and Technology (GIST), Buk-gu, Gwangju, 61005, South Korea

ARTICLE INFO

Keywords:
Metal organic framework
Grand canonical Monte Carlo
Machine learning
Ammonia capture

ABSTRACT

Ammonia (NH₃) has been a subject of great interest due to its important roles in diverse technological applications. However, high toxicity and corrosiveness of NH₃ has made it an important task to develop an efficient carrier to safely capture NH₃ with high capacity. Here, we employ a machine learning (ML) model to discover high-performance metal organic frameworks (MOFs) that will work as efficient NH₃ carriers. By constructing databases at two distinct conditions, adsorption and desorption, through Grand Canonical Monte Carlo (GCMC) simulations to train ML models, we identify eight novel MOFs as potentially efficient NH₃ carriers through screening the large-scale MOF databases with the trained models and GCMC verification. The identified MOFs exhibit the average NH₃ working capacity exceeding 1100 mg/g, and subsequent molecular dynamics simulations demonstrate mechanical stability of the predicted MOFs. Moreover, analyses of the diffusion mechanism within the proposed MOFs underscore the strong dependence of NH₃ gas diffusivity on the structural details of the materials.

1. Introduction

Ammonia (NH₃) is a colorless gas that plays a pivotal role in various technological domains such as refrigeration, fertilizer production, and manufacturing synthetic fibers and plastics [1–4]. Despite the widespread utilization, the safe handling of NH₃ remains as a complex challenge due to its intrinsic toxicity and corrosive nature, and ensuring the safety of both workers and the environment thus necessitates a meticulous approach to treatment and storage of the gas. A critical aspect of securely storing NH₃ gas involves the identification of a material capable of containing NH₃ without undergoing reactions or degradation over time [5–7]. An optimal storage material is expected to exhibit resilience to high pressures and temperatures, resist corrosion and abrasion, and prevent gas leakage. Although conventional materials including resins [8], zeolites [9] and mesoporous silica [10] show promise as NH₃ carriers, the burgeoning demand for NH₃ underscores the ongoing pursuit of outstanding storage solutions.

In this context, metal-organic frameworks (MOFs), characterized by metal ions or clusters interconnected with organic ligands, have emerged as promising candidates for efficient gas storage due to their appealing attributes such as high porosity, large pore-surface area, tunability and stability [11-15], and recent studies have indeed

elucidated high performance of MOFs in storing NH₃ gas [16–19]. One of the advantages of MOFs lies in the configurational diversity between metal ions and linkers which enables the optimization of properties, including adsorption capacity and stability [20]. Liu et al. have examined various MOFs for NH3 adsorption capacity and structural stability, including MIL-101 whose NH3 adsorption capacity records 700 mg/g at 303 K and 6.1 bar [21], and even higher adsorption capacity of 760 mg/g has been reported for MIL-101 at 298 K and over 5 bar [22]. Also, computational screening finds appropriate ligands to construct MOF-303 (Al) which shows 335.5 mg/g for the NH₃ adsorption capacity at at 25.0 °C and 1.0 bar [23]. Rieth et al. have studied on stable triazolate frameworks with open metal sites and found that the NH3 adsorption capacity of Co₂Cl₂BBTA reaches 145.8 mg/g at 1000 ppm of $\mathrm{NH_{3}},$ which is higher than that of the state-of-the-art HKUST-1 by 27 %[24]. Interestingly, it should be noted that under conditions of room temperature and high pressure exceeding 5 bar, MIL-101 achieves a density nearly half that of liquid ammonia (681.9 kg/m³ at 240 K) [22, 25].

While these results are interesting and promising, possibilities still exist to discover MOFs with further enhanced NH_3 adsorption capacity, especially within narrow temperature range around room temperature and at an elevated pressure, but the expansive search space resulting

E-mail address: jhyoung@gist.ac.kr (J.-H. Lee).

^{*} Corresponding author.

from myriad constituent combinations within MOFs poses a formidable challenge for determining proper candidate materials possessing satisfactory NH₃ adsorption performance. In this work, we employ a machine learning (ML) model to expedite the identification of MOFs with high NH3 working capacity. Trained with a database generated via Grand Canonical Monte Carlo (GCMC) simulations, the ML model rapidly evaluates more than 12,000 MOFs in the Computation-Ready Experimental Metal Organic Framework (CoRE MOF) database [26] and, combined with GCMC calculations, identifies promising MOFs with high NH₃ working capacity. Intriguingly, the selected MOFs exhibit type IV or V isotherms [27], showcasing high working capacities within narrow temperature range (20K) near room temperature. This characteristic offers advantages for both efficient NH3 gas transport and reducing the cycling time. In addition to ML screening and GCMC computations, molecular dynamics (MD) simulations are conducted to analyze diffusion processes. This step is crucial for understanding gas diffusivities within the proposed MOFs, providing valuable insights into their potential for various applications involving NH₃ gas.

2. Methods

2.1. Machine learning

All MOF data including structural information and material properties used for constructing a database are collected from the Materials Project (MP) MOF explorer [28-30] and CoRE MOF database. 1290 MOFs together with their atomic charge information are retrieved from the MP MOF database, and the NH3 adsorption capacities of each MOF are calculated by GCMC simulations. The obtained dataset is then split into the train and test datasets with 85 % and 15 % ratio to train a ML model and evaluate the model performance, respectively. The feature vectors for the ML model, as is implemented within a neural network (NN) scheme, are composed of eight geometric descriptors of MOFs and a one-hot encoded metal component. Geometric descriptors of MOFs include the largest cavity diameter (LCD) (Å), pore-limiting diameter (PLD) (Å), largest free path diameter (LFPD) (Å), density (g/cm³), volumetric surface area (VSA) (m²/cm³), gravimetric surface area (GSA) (m²/g), void fraction (VF) and accessible volume (AV) (cm³/g), which are available from CoRE MOF database. The metal element is one-hot encoded with element 1 at the position of its atomic number and the rest being 0.

2.2. GCMC and electronic structure calculations

The NH₃ adsorption capacity of MOFs is calculated through GCMC simulations which are carried out with RASPA 2.0 code [31]. The GCMC simulations are first performed on MOF data to construct an in-house database for ML training, and afterwards to validate the predicted results by the ML model. It is noted that all the atoms within MOFs are assumed to be immovable during the simulation processes. The interactions between atoms within the MOFs and those within NH₃ molecules are described by the Lennard-Jones (LJ) potentials in the Universal Force Field (UFF) [32] and Transferable Potentials for Phase Equilibria (TraPPE) force field (Table S1 in Supporting Information, SI) [33], respectively. For the interaction between MOFs and adsorbed NH₃ molecules, the Lorentz-Berthelot mixing rule with the LJ potential is employed [34]. Since all atoms are considered as charged, the Coulomb interaction is properly treated within Ewald scheme [31].

To address the LJ interactions, the spherical cutoff of 14 Å together with analytic tail correction is adopted. In the GCMC simulations, the atomic charge data is collected from the MP database for constructing the MOF databases to train the ML model and is computed through density functional theory (DFT) calculations for validating the screened properties, respectively. It should be noted that DFT calculations are conducted by employing SIESTA [35] package with the density derived electrostatic and chemical approach [36] and generalized gradient

approximation [37] for the exchange-correlation interaction among electrons. The GCMC simulations are performed with five different types of Monte Carlo moves that have equal probability including translations, rotations, insertions, deletions and reinsertion. For constructing the dataset, the simulation runs 7500 cycles for equilibration and another 7500 cycles to obtain the NH3 adsorption performance of MOFs, and subsequently to screen for high performance MOFs, the simulation runs 2×10^4 cycles for equilibration, which is followed by additional 2×10^4 cycles for production of the absolute adsorption amount of NH3 gas. All simulations are separately performed under adsorption (293K, 5 bar) and desorption conditions (313K, 5 bar).

2.3. MD simulations

MD simulations are performed with LAMMPS code [38] to calculate bulk modulus and examine the diffusion behavior of NH $_3$ gas molecules within the proposed MOFs. The time step is set to be 0.1fs and the interatomic interactions are treated in the same manner as in the GCMC simulations. The number of NH $_3$ molecules in a simulation box is determined from the GCMC simulation results of each MOF at the adsorption condition. After equilibrating for 1ns at 293K using the Nose-Hoover thermostat, the NH $_3$ diffusion is simulated for 2.5ns within the NVT ensemble. During the simulations, the mean square displacements (MSD) of all ammonia molecules are collected from the molecules' trajectories which are recorded every 0.1ps and averaged for multiple time intervals. The diffusivity of NH $_3$ gas molecules inside MOFs is then calculated by taking a temporal gradient of MSD.

3. Results and discussion

3.1. GCMC simulations

In order to assess the validity of the present GCMC simulations, we first compare the results from our GCMC simulations for MIL-101 with available experiment [22,39]. As is seen from Fig. 1(a), which shows the isotherms of the NH₃ adsorption capacity at 298K, the simulation results agree very well with experiment under 4 bar. At higher pressures, however, the GCMC simulations tend to overestimate the NH3 adsorption capacity, which can be attributed to several factors. Firstly, in the GCMC simulations MOFs are assumed to be rigid with unchanging pore volumes, possibly resulting in higher adsorption capacities compared to actual MOFs, particularly under high-pressure conditions. Secondly, the assumption of uniform distribution of ammonia molecules inside MOF in simulations may not properly reflect actual experimental conditions. Nonetheless, both experimental and simulated adsorption isotherms exhibit nearly the same variation with pressure, which validates the GCMC simulations for investigating the adsorption properties of NH₃ in MOFs. Moreover, Liu et al. have shown that despite an overestimation by approximately 40 % in the simulated NH3 adsorption capacities of MIL-101 and NU-1000 compared to their experimental results, the GCMC simulations effectively capture the essence of experimental outcomes [21].

3.2. Screening MOFs with machine learning

To predict the NH_3 adsorption capacity of MOFs with a ML model, we first generate a MOF dataset by carrying out GCMC simulations as previously described. The initial dataset is found to contain no MOF counts in the high-capacity range (Fig. S1(a) in SI), which would result in severely biased and inaccurate predictions. To circumvent this situation, the dataset is augmented with 104 additional MOFs which are selected from CoRE MOF database and predicted to show high NH_3 adsorption capacity through combined pre-trained ML and GCMC simulations. The enlarged dataset contains a finite number of MOFs which show high NH_3 adsorption capacity exceeding $1000 \ mg/g$ (Fig. S1(b) in SI).

Fig. 1(b) and (c) illustrate the performance of the trained NN-based

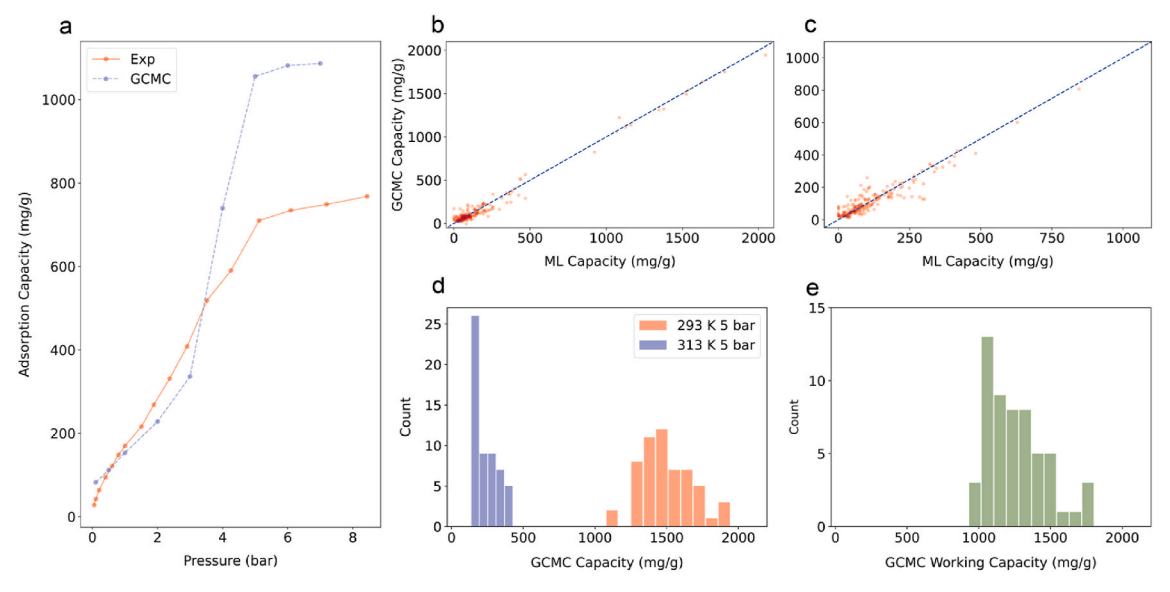


Fig. 1. (a) The isotherm comparison between the GCMC simulation and experiment [22,39] for MIL-101 at 298 K. Training performance of the ML model at (b) adsorption (293K, 5 bar) and (c) desorption (313K, 5 bar) conditions, respectively. (d) MOF distributions with respect to the NH₃ adsorption capacity at both conditions, and (e) the working capacity.

ML model against the test set at the adsorption and desorption conditions, respectively. Comparing to the results of GCMC simulations, it is found that the ML-predicted values present $R^2=0.978$ (0.862) with 33.49 (28.14) mg/g of the mean absolute error (MAE) in the adsorption (desorption) environment. Notably, while the MAEs are similar in both cases, R^2 for the desorption is lower than that for the adsorption condition. This reduction in R^2 is attributed primarily to the low pressure of the desorption state $p/p_0=0.32$, where p_0 is the saturation pressure of NH₃ at a given temperature, as opposed to $p/p_0=0.56$ under the adsorption condition.

To assess the NH₃ adsorption performance, we apply the trained ML model to the CoRE MOF database which contains more than 12,000 MOFs and subsequently validate the ML-predicted results through GCMC simulations. For comparison purposes, MIL-101 is taken as a reference MOF which is one of the most well-studied materials for NH3 adsorption. With MIL-101, GCMC simulations yield 1087.06 and 369.38 mg/g for the NH₃ adsorption capacities at 293K and 313K, respectively, resulting in 717.68 mg/g for the working capacity, the capacity difference between the two temperatures. Taking 900 mg/g as a target working capacity, which is 20 % higher than the MIL-101 value, we first identify 56 MOFs whose distribution at each condition is given in Fig. 1 (d). As is seen from Fig. 1(d), the adsorption capacity ranges from 1073 to 1944 mg/g with 1492 mg/g on average at 293K, and the distribution is rather symmetric around the average adsorption capacity, showing a Gaussian-like envelope. In contrast, the result at 313K displays a highly left-biased distribution with a narrow range between 135 and 427 mg/g. In particular, it is found that nearly 50 % of the MOFs have the adsorption capacity lower than 200 mg/g at 313K, which then leads to an asymmetric distribution of the working capacity as is shown in Fig. 1 (e). As is seen from Fig. 1(e), the working capacity ranges from 928 to 1805 mg/g with average of 1259 mg/g, and nearly 90 % of the MOFs have their capacity less than 1500 mg/g.

3.3. Feature importance

Before final screening of potential MOFs for efficient NH_3 capture, it is instructive to analyze how much each feature contributes to the NH_3 adsorption performance. To this end, the feature importance of the ML model is calculated based on the permutation importance algorithm (PIA). In PIA, the values of each feature column are randomly shuffled, and the score of the ML model (R^2) is evaluated thereafter. The

importance of each feature is then determined from the change in the R^2 value compared to the original model [40]. Specifically, for the i-th feature the score difference $\Delta_i = R_i^2 - R_0^2$, where R_i^2 and R_0^2 are the model scores with and without random shuffling, respectively, is calculated and the relative importance of the *i*-th feature (ρ_i) is quantified as $\rho_i = \Delta_i / \sum_i \Delta_i$ with summation being carried out over all features. The larger ρ_i values implies that the corresponding feature plays a more important role in producing the result. Fig. 2(a) shows the obtained relative feature importance of the nine descriptors (LCD, PLD, LFPD, density, VSA, GSA, VF, AV and metal atoms) at the adsorption and desorption conditions, respectively. As is seen from Fig. 2(a)-AV, PLD and GSA are the most influential properties in determining the materials performance in that the average importance is 0.19 and 0.18 at 293K and 313K, respectively, which is 70 % higher than the next three decisive features (LFPD, VSA, LCD). The significance of PLD can be understood from the observation that MOFs with PLD less than the kinetic diameter of NH3 molecules display the poor adsorption performance [41]. Also, AV and GSA have strong effect on the adsorption performance because high AV and GSA makes more atomic sites within MOFs available for adsorption.

Further insight into the relation between the structural parameters and NH3 adsorption performance can be achieved by examining the distribution of the working capacity with respect to the three most important features, PLD, GSA and AV, as is illustrated in Fig. 2(b-g). In Fig. 2(b), the adsorption capacity at 293K tends to increase with PLD and reaches a maximum around 13 Å below which most MOFs are present. For PLD larger than 13 Å, the adsorption capacity shows a rapid decrease. At the higher temperature, the calculated capacity exhibits nearly the same behavior except the maximum which is shifted to PLD~10 Å. The decrease in the adsorption capacity at high PLD values can be attributed to the point that larger PLD corresponds to expanded pore dimensions, which would reduce the fraction of ammonia molecules near the pore surface and thus lower the scattering rate. Enhanced pressure could contribute to maintaining the adsorption capacity by compensating the decreased scattering between NH3 and the surface. Combining the adsorption capacities at the two temperatures, the working capacity is appreciable only for PLD>10 Å, as is illustrated in

In Fig. 2(c), the adsorption capacity of MOFs is shown to increase with the GSA until the GSA becomes close to $3000\ m^2/g$. For the GSA

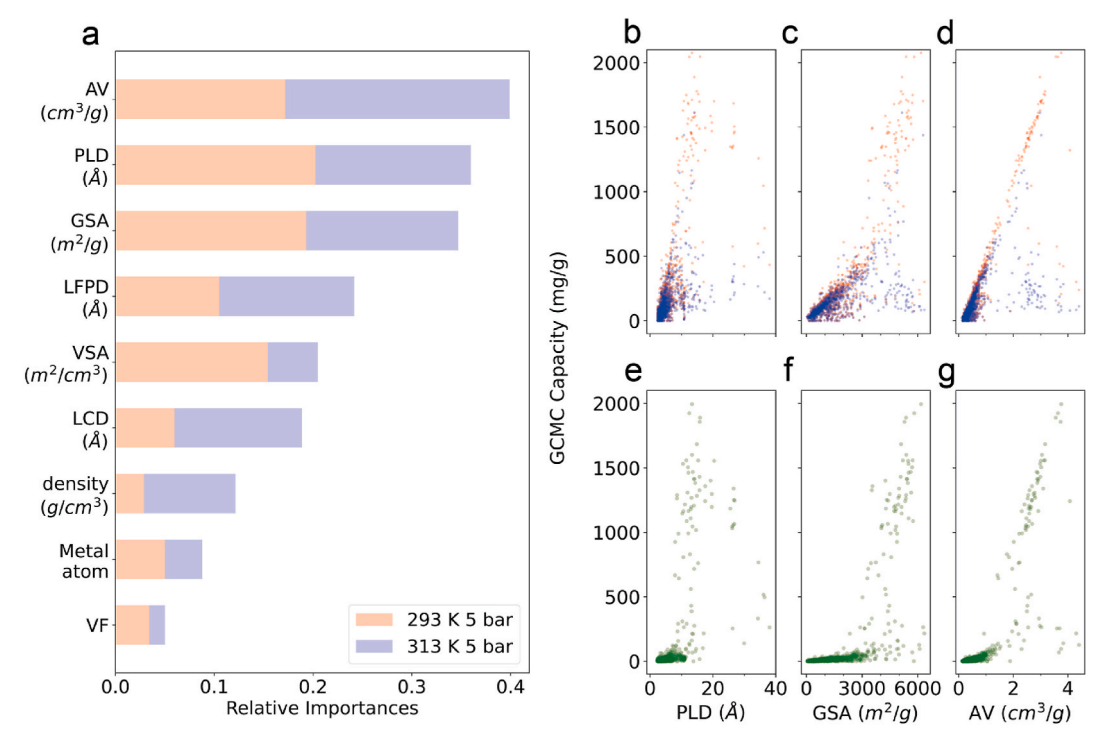


Fig. 2. (a) Relative feature importance of the MOF descriptors. The red and blue bars represent the relative importance at adsorption and desorption conditions, respectively. (b–g) The relationship between the three most important descriptors and NH_3 adsorption capacities: (b, e) PLD (Å), (c, f) AV (cm³/g) and (d, g) GSA (m²/g). In (b)–(d), red and blue circles represent the GCMC simulation results at the adsorption desorption conditions, respectively. Green circles in (e)–(g) represent the working capacity.

higher than 3000 m²/g, the adsorption capacity continues to increase at the adsorption condition, whereas it decreases at the desorption condition. As for the AV, the adsorption capacity of MOFs displays a strong linear dependence on the AV as is depicted in Fig. 2(d), and the primary difference between the two temperatures is the AV value around which the adsorption capacity begins to decrease. At 313K, it occurs AV~2.0 cm³/g and the corresponding value for the low temperature is much higher. Due to the similar behavior in the adsorption capacity at 293K and 313K with respect to GSA and AV, the working capacity becomes appreciable only when GSA \gtrsim 3000 m [2]/g (Fig. 2(f)) and AV \gtrsim 2.0 cm³/g (Fig. 2(g)), respectively. For the other structural features, the adsorption performance is relatively similar to those of the PLD, GSA and AV (see Fig. S2 in SI). In cases of LFPD (Figs. S2(a) and (f) in SI), VSA (Figs. S2(b) and (g) in SI) and LCD (Figs. S2(c) and (h) in SI), the low- and high-temperature adsorption capacities becomes appreciably different only when the feature values become large, which is particularly pronounced for VF as is presented in Figs. S2(e) and (j) in SI. The working capacity shows an abrupt increase around VF~0.8. However, the NH₃ adsorption characteristic is opposite for density as is seen from Figs. S2 (d) and (i) in SI, where the working capacity sharply decreases and becomes less than 100 mg/g when the density is higher than 0.5 cm³/g. The reason for such difference is that all the other descriptors are related with cavity or pore region within MOFs, and larger values of those features imply that more ammonia molecules can be accommodated inside MOFs, thus leading to higher working capacity in general. In cases of density, however, increased void fraction within MOFs results in decreased density, making low-density MOFs more advantageous for adsorbing NH3 molecules.

3.4. Properties of the selected MOFs

Since all MOFs in the present study are assumed to be rigid and immovable during GCMC simulations [31], the mechanical stability of the MOFs needs to be examined in addition to the NH₃ working capacity.

To this end, we compute bulk modulus (B) of each MOF with MD simulations by employing LAMMPS code [38] with UFF [32] since B is considered as a useful metric to gauge mechanical stability [42]. Taking the bulk modulus of MIL-101 as a lower bound (10.06 GPa), we finally select eight MOFs for efficiently carrying ammonia molecules. The crystal structures of the selected MOFs are presented in Fig. 3 together with their Cambridge Structural Database (CSD) Refcodes and the physical properties of the MOFs are listed in Table 1, respectively. In Fig. 3, it should be noted that PIBNUK and PIBNUK01 are structurally very close since they are optical isomers and the difference between WUHCUZ and WUHDAG is organic ligands connecting metal elements (the situation is the same for MERLAZ and MERLED pair). As is seen from Table 1, the average working capacity and bulk modulus of the candidate MOFs are 1168.84 mg/g and 11.82 GPa, respectively, and the maximum values are 1533.35 mg/g and 13.8 GPa for each property, which are 113.6 % and 37.2 % higher than the corresponding values of MIL-101.

It is noted that further insights can be gained by examining the adsorption isothermal graphs for the final MOFs which will provide the pressure dependence of NH₃ adsorption performance. As is presented in Fig. 4(a), the adsorption capacity at 293K is nearly the same for most MOFs: it slowly increases from 100 mg/g or so and shows an abrupt jump to higher values between 3 and 4.5 bar, resulting in type V adsorption isotherms. Such low capacity at low pressure is due to the weak interaction between the MOF surfaces and NH3 molecules, arising from the hydrophobicity of organic linkers, which requires higher pressure of NH₃ for efficient pore filling. This is also in line with the observation that the pressure at which the adsorption capacity exhibits a sharp upturn increases with LCD of MOFs (Table 1). At elevated pressures, on the other hand, the MOFs can be grouped into three different classes according to their saturated working capacities: (i) around 1000 mg/g (PIBNUK, PIBNUK01), (ii) between 1200 and 1300 mg/g (AWU-PAL, YODWOF, MERLAZ, MERLED) and (iii) more than 1500 mg/g (WUHCUZ, WUHDAG). This difference in the high-pressure adsorption

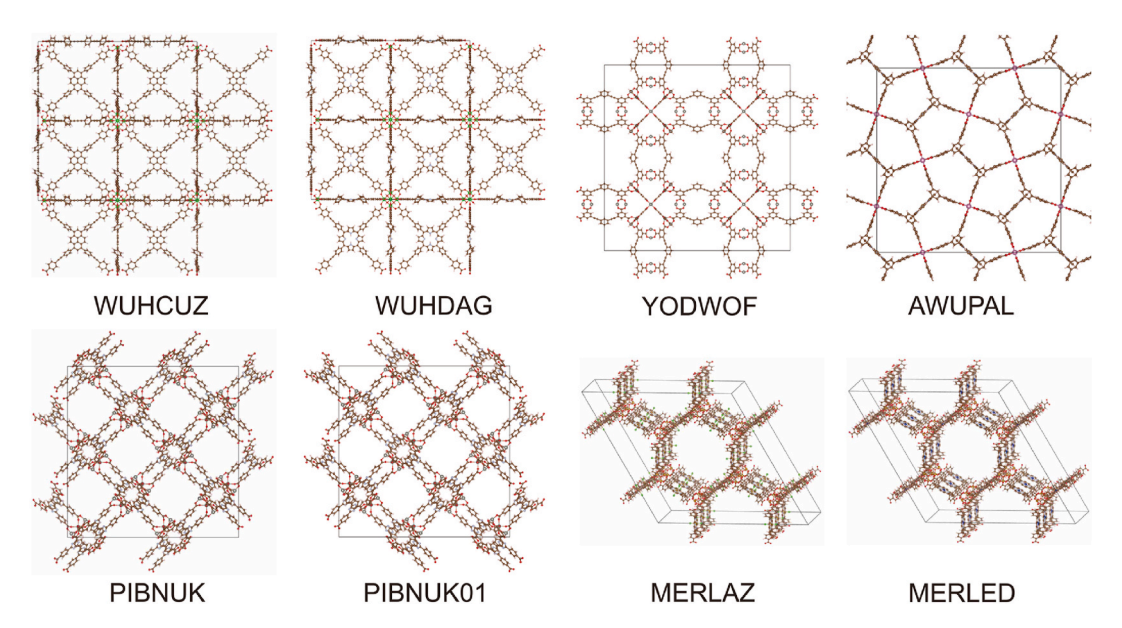


Fig. 3. The crystal structures of the selected MOFs with high working capacity and bulk modulus.

Table 1Physical properties of the selected MOF candidates.

CSD code	Bulk moduli (GPa)	Calculated adsorption capacity (mg/g)			Metal	LCD	PLD
		293 K 5 bar (a)	313 K 5 bar (b)	(a-b)			
WUHCUZ [44]	13.8	1607.12	102.37	1504.75	Zr	23.13	12.21
WUHDAG [44]	13.5	1631.27	97.92	1533.35	Zr	25.24	10.50
YODWOF [45]	12.83	1372.41	358.38	1014.03	Zn	21.60	14.64
AWUPAL [46]	11.7	1352.17	174.39	1177.78	In, Fe	18.42	9.24
PIBNUK01 [47]	11.02	1065.64	146.05	919.59	Zn	15.37	14.18
PIBNUK [47]	10.92	1075.49	147.24	928.25	Zn	15.38	14.19
MERLAZ [48]	10.45	1358.64	165.35	1193.29	Fe, Co	27.21	25.55
MERLED [48]	10.32	1252.62	172.92	1079.70	Fe	27.34	23.18

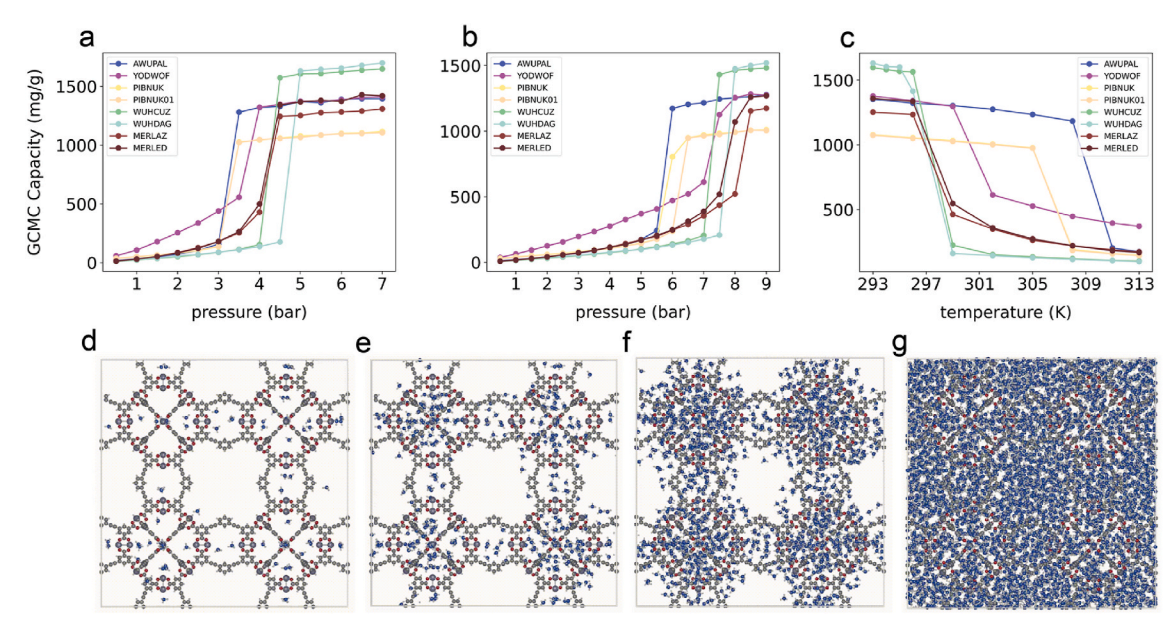


Fig. 4. The isotherm graph for the eight selected MOFs at (a) 293 K and (b) 313 K. (c) The isobaric graph for the best eight MOFs at 5 bar. Snapshots of GCMC simulations of YODWOF with increasing pressure: (c) 0.1 bar, (d) 1 bar, (e) 3 bar and (f) 5 bar.

capacity is attributed to the structural dissimilarity of the MOFs. As is illustrated in Fig. 3, the structures of PIBNUK and PIBNUK01 are nearly identical except for mirror reflection and the organic ligands

differentiate WUHCUZ (MERLAZ) from WUHDAG (MERLED). It is also interesting to observe in Fig. 4(b) that the upturn pressure is shifted to higher values than lower temperature cases, which is for compensation

of enhanced thermal effect on NH_3 molecules. In Fig. 4(c), the isobaric graphs of the NH_3 adsorption capacity are presented for the eight MOFs at 5 bar, which show the decrease in the adsorption capacity as temperature increases. Interestingly, the adsorption capacity sharply changes within narrow temperature range, which will be advantageous in reducing the time required for regeneration cycles. Since a considerable amount of time is typically needed in adsorption/desorption cycles of NH_3 molecules when commercially available methods are employed, the proposed MOFs are expected to expedite the regeneration cycles.

It should be noted that the low-pressure absorption capacity YOD-WOF shows higher values than those of the other MOFs at both temperatures, resulting in type IV isotherm, which can be understood from structural consideration. As is shown in Fig. 3, YODWOF consists of two different sizes of pore, smaller ones having several binding sites and larger ones with high surface area. Such hierarchical porous structures make smaller pores filled first at lower pressures. Fig. 4(d)–(g) shows the snapshots of GCMC simulations at 293K for YODWOF at different pressures. When the pressure is less than 3 bar, NH₃ molecules begin to fill smaller pores first (Fig. 4(d)–(f)) and larger pores are filled only after the pressure is increased to 5 bar (Fig. 4(g)).

3.5. Diffusion process of NH3 molecules

When studying NH_3 adsorption within MOFs, a large number of ammonia molecules are considered in a unit cell, which would result in reduced mean free path of NH_3 molecules and gas diffusivity. In contrast, MOFs in experiment will have more gas molecules near the surface than inside the bulk, and it is thus necessary to investigate the gaseous transport characteristics within MOFs by taking high NH_3 gas

loading into account. To this end, we carry out MD simulations by matching the $\rm NH_3$ gas loading in each MOF to the number of gas molecules employed in GCMC simulations.

Fig. 5(a) presents the mean square displacement (MSD) of the eight MOFs at 293K as a function of time after 1ns of equilibration. Since the MSD linearly increases with time as is clear from Fig. 5(a), and the diffusivity (D) can be easily estimated from the slope of the MSD line. It is seen from the figure that PIBNUK and WUHDAG possess the highest and lowest D values of 1.9×10^{-8} m²/s and 3.7×10^{-9} m²/s, respectively. In general cases, the PLD has a strong effect on the gaseous diffusivity in that D shows sharp decrease when the PLD is smaller than the kinetic diameter of gas molecules ($d_{\rm kin}$) whereas it monotonically increases if PLD > $d_{\rm kin}^4$. In the present cases, however, the correlation between the PLDs and diffusivity of the proposed MOFs is weak as is shown in Fig. 5(b) because the PLDs of the MOFs are already higher than $d_{\rm kin}$ of NH₃ molecules, and the LCD also has a weak correlation with D (Fig. 5(b)).

However, Fig. 5(c) reveals that the NH₃ diffusivity of the MOFs displays a strong negative correlation with the LCD-to-PLD ratio. Notably, diffusion occurring between the cages of the MOFs exerts more substantial influence on both MSD and diffusivity than diffusion within a single cage, implying that active inter-cage jump positively correlates with higher diffusivity. Conversely, a smaller LCD/PLD value results in less frequent inter-cage jumping events, which will lead to a reduction in diffusivity. Thus, in cases of high NH₃ gas loading, the ratio between the LCD and PLD plays a crucial role in determining the gaseous transport characteristics.

For comparison purposes, we also compute the diffusivity under desorption condition. In cases of desorption, the number of gas molecules is generally lower than that of the adsorption cases, which

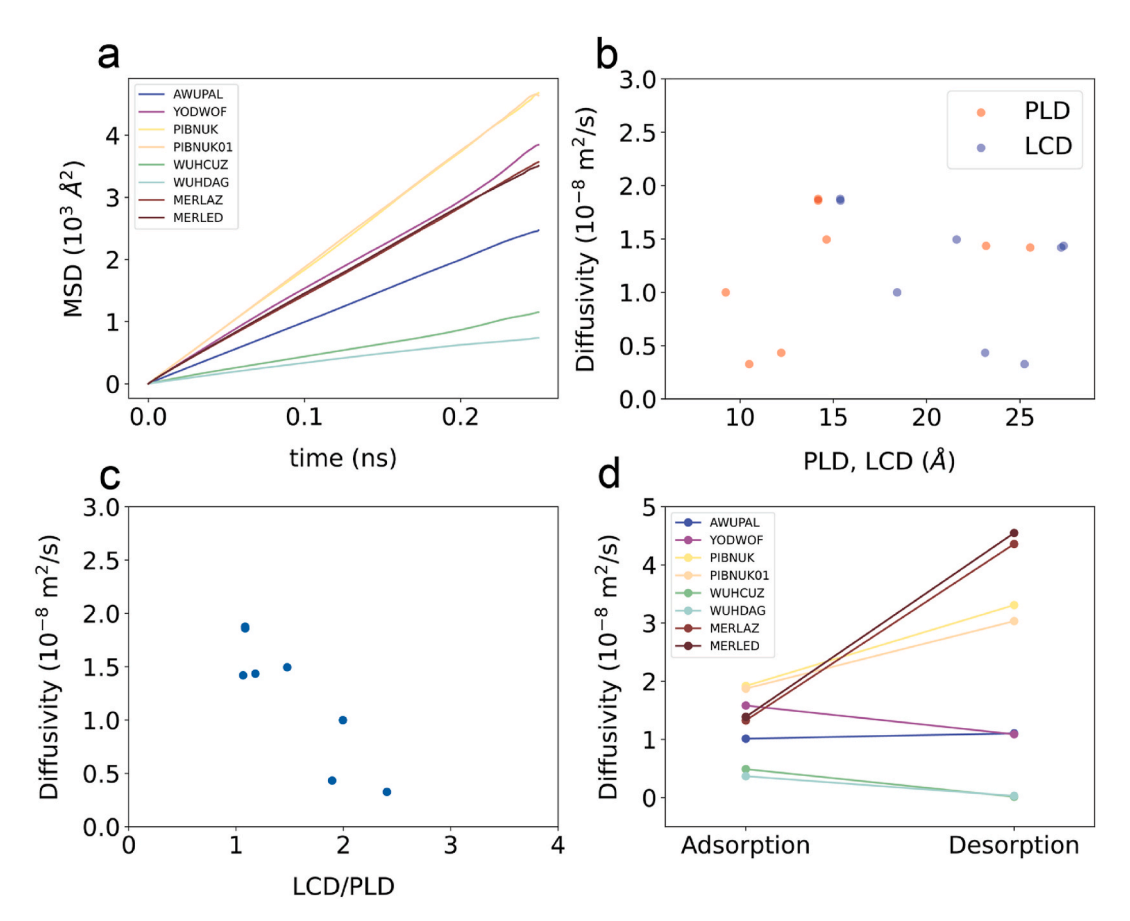


Fig. 5. (a) The time-dependent MSDs of the selected MOFs. The MSDs during 2.5 ns are recorded after 1 ns equilibration. Their diffusivities are obtained from the gradient of the time-MSD line. The relationship between MSD, (b) PLD (red), LCD (blue) and (c) LCD/PLD are plotted. (d) The diffusivity difference between adsorption condition and desorption condition.

typically leads to an increase in gaseous diffusivity due to steric effects. The diffusivities are compared in Fig. 5(d) between the adsorption and desorption conditions. As is shown in Fig. 5(d), while WUHCUZ and WUHDAG show very limited diffusion under the desorption conditions since they contain a small number of NH $_3$ gas molecules within a unit cell which are strongly bound to the adsorption sites, PIBNUK, PIBNUK01, MERLAZ and MERLED exhibit an increase in diffusivity in desorption cases. And AWUPAL and YODWOF display minimal change and slight decrease in the diffusivity, respectively, under the desorption conditions, which is primarily due to the small cage effect.

The small cage effect arises from the observation that inter-cage jumps between large pores are more active than between pores with dissimilar sizes, which allows for freer diffusion of gas molecules in larger pores while confining them in smaller pores. At high gas loading, in particular, the frequency of escaping from small cages due to interactions with external gas molecules is relatively high, but such escaping is reduced as gas loading decreases, causing diffusivity to increase at elevated gas loading [43]. As previously mentioned, YODWOF possesses a hierarchical pore configuration and exhibits a tendency to fill smaller pores first, which brings about lower diffusivity under the desorption condition due to the small cage effect. In cases of AWUPAL, the PLD is low compared to LCD, which leads to the decreased pore entrance, and the small cage effect is competing with steric effect, making almost no difference in diffusivity regardless of temperature.

4. Conclusion

In the present study, we have proposed novel MOFs which would possess high NH₃ adsorption performance by employing a combined MLaided screening and GCMC simulations. Although the ML model takes its most inputs from simple geometric parameters of the MOFs, the model performance is highly satisfactory as is evidenced by the R^2 value. Moreover, by analyzing the feature importance, the available volume and pore-limiting diameter are the two most important factors in determining the NH3 adsorption performance. Considering two operation temperatures, 293K and 313K, it is possible to identify eight potential MOFs with high NH3 working capacity, which exceeds the corresponding values of previously studied MOFs. The gaseous diffusivity is also a critical attribute that significantly affects the adsorption performance of the materials. During the regeneration cycles, the gaseous diffusivity experiences alterations in response to variations in the amount of adsorbed gas molecules. In typical MOFs, which are primarily influenced by steric effects, higher gaseous diffusivities are observed at lower gas loadings. However, when the small cage effect becomes stronger, the corresponding gaseous diffusivity is found to be lower at lower gas loadings. These findings show a promise of an MLaided approach in accelerated search for novel MOFs for gas adsorption applications. Moreover, our results demonstrate that geometric information of MOFs are crucial in determining adsorption performance, which will be advantageous for structural engineering to design highperformance MOFs.

CRediT authorship contribution statement

Sanghyun Kim: Writing – review & editing, Writing – original draft, Investigation, Formal analysis, Data curation, Conceptualization. **Joo-Hyoung Lee:** Writing – review & editing, Supervision, Resources, Investigation, Funding acquisition, Formal analysis, Conceptualization.

Declaration of competing interest

The authors declare that they have no known competing financial interests or personal relationships that could have appeared to influence the work reported in this paper.

Data availability

Data will be made available on request.

Acknowledgements

This work was supported by the Korea Institute of Energy Technology Evaluation and Planning (KETEP) grant funded by the Korean Government (20212050100010) and the National Research Foundation of Korea (RS-2023-00253716).

Appendix A. Supplementary data

Supplementary data to this article can be found online at $\frac{\text{https:}}{\text{doi.}}$ org/10.1016/j.mtadv.2024.100510.

References

- H. von Blottnitz, M.A. Curran, A review of assessments conducted on bio-ethanol as a transportation fuel from a net energy, greenhouse gas, and environmental life cycle perspective, J. Clean. Prod. 15 (2007) 607–619.
- [2] E. Martínez-Ahumada, M.L. Díaz-Ramírez, M. de J. Velásquez-Hernández, V. Jancik, I.A. Ibarra, Capture of toxic gases in MOFs: SO₂, H₂S, NH₃and NO_x, Chem. Sci. 12 (2021) 6772–6799.
- [3] K. Vikrant, V. Kumar, K.H. Kim, D. Kukkar, Metal-organic frameworks (MOFs): potential and challenges for capture and abatement of ammonia, J. Mater. Chem. A 5 (2017) 22877–22896.
- [4] C.D. Demirhan, W.W. Tso, J.B. Powell, E.N. Pistikopoulos, Sustainable ammonia production through process synthesis and global optimization, AIChE J. 65 (2019).
- [5] K.V. Kumar, K. Preuss, M.M. Titirici, F. Rodríguez-Reinoso, Nanoporous materials for the Onboard storage of natural gas, Chem. Rev. 117 (2017) 1796–1825.
- [6] R.E. Morris, P.S. Wheatley, Gas storage in nanoporous materials, Angew. Chemie-Int. Ed. 47 (2008) 4966–4981.
- [7] K.A. Cychosz, M. Thommes, Progress in the physisorption characterization of nanoporous gas storage materials, Engineering 4 (2018) 559–566.
- [8] J. Helminen, J. Helenius, E. Paatero, I. Turunen, Adsorption Equilibria of ammonia gas on inorganic and organic sorbents at 298.15 K, J. Chem. Eng. Data 46 (2001) 391–399.
- [9] J. Helminen, J. Helenius, E. Paatero, I. Turunen, Comparison of sorbents and isotherm models for NH3-gas separation by adsorption, AIChE J. 46 (2000) 1541–1555.
- [10] A.M.B. Furtado, Y. Wang, T.G. Glover, M.D. LeVan, MCM-41 impregnated with active metal sites: synthesis, characterization, and ammonia adsorption, Microporous Mesoporous Mater. 142 (2011) 730–739.
- [11] H. Furukawa, K.E. Cordova, M. O'Keeffe, O.M. Yaghi, The chemistry and applications of metal-organic frameworks, Science 341 (2013).
- [12] U. Mueller, et al., Metal-organic frameworks prospective industrial applications, J. Mater. Chem. 16 (2006) 626–636.
- [13] S. Horike, S. Shimomura, S. Kitagawa, Soft porous crystals, Nat. Chem. 1 (2009) 695–704.
- [14] G. Maurin, C. Serre, A. Cooper, G. Férey, The new age of MOFs and of their porousrelated solids, Chem. Soc. Rev. 46 (2017) 3104–3107.
- [15] H.C.J. Zhou, S. Kitagawa, Metal-organic frameworks (MOFs), Chem. Soc. Rev. 43 (2014) 5415–5418.
- [16] D. Saha, S. Deng, Ammonia adsorption and its effects on framework stability of MOF-5 and MOF-177, J. Colloid Interface Sci. 348 (2010) 615–620.
- [17] Y. Chen, et al., Zirconium-based metal-organic framework with 9-connected nodes for ammonia capture, ACS Appl. Nano Mater. 2 (2019) 6098–6102.
- [18] Y. Chen, et al., Recyclable ammonia uptake of a MIL series of metal-organic frameworks with high structural stability, Microporous Mesoporous Mater. 258 (2018) 170–177.
- [19] C. Petit, T.J. Bandosz, Enhanced adsorption of ammonia on metal-organic framework/graphite oxide composites: analysis of surface interactions, Adv. Funct. Mater. 20 (2010) 111–118.
- [20] T. Kajiwara, et al., A systematic study on the stability of porous coordination polymers against ammonia, Chem. Eur J. 20 (2014) 15611–15617.
- [21] Z. Liu, et al., The potential use of metal-organic framework/ammonia working pairs in adsorption chillers, J. Mater. Chem. A 9 (2021) 6188–6195.
- [22] G. An, et al., Metal-organic frameworks for ammonia-based thermal energy storage, Small 17 (2021) 1–11.
- [23] Z. Wang, et al., Tailoring multiple sites of metal-organic frameworks for highly efficient and reversible ammonia adsorption, ACS Appl. Mater. Interfaces 13 (2021) 56025–56034.
- [24] A.J. Rieth, M. Dincă, Controlled gas uptake in metal-organic frameworks with record ammonia sorption, J. Am. Chem. Soc. 140 (2018) 3461–3466.
- [25] D.M. Yost, Systematic Inorganic Chemistry, Read Books, 2007.
- [26] Y.G. Chung, et al., Advances, updates, and analytics for the computation-ready, experimental metal-organic framework database: CoRE MOF 2019, J. Chem. Eng. Data 64 (2019) 5985–5998.

- [27] S. K.S.W, et al., Reporting physisorption data for gas/solid systems with special reference to the determination of surface area and porosity, Pure Appl. Chem. 57 (1985)
- [28] A. Jain, et al., Commentary: the Materials Project: a materials genome approach to accelerating materials innovation, Apl. Mater. 1 (2013) 011002.
- [29] A.S. Rosen, et al., Machine learning the quantum-chemical properties of metal-organic frameworks for accelerated materials discovery, Matter 4 (2021) 1578–1597.
- [30] A.S. Rosen, et al., High-throughput predictions of metal-organic framework electronic properties: theoretical challenges, graph neural networks, and data exploration, npj Comput. Mater. 8 (2022).
- [31] D. Dubbeldam, S. Calero, D.E. Ellis, R.Q. Snurr, RASPA: molecular simulation software for adsorption and diffusion in flexible nanoporous materials, Mol. Simul. 42 (2016) 81–101.
- [32] A.K. Rappe, C.J. Casewit, K.S. Colwell, W.A. Goddard, W.M. Skiff, UFF, a full periodic table force field for molecular mechanics and molecular dynamics simulations, J. Am. Chem. Soc. 114 (1992) 10024–10035.
- [33] L. Zhang, J.I. Siepmann, Development of the Trappe Force Field for Ammonia, 2010 at
- [34] M.P. Allen, et al., Computer Simulation of Liquids, reprint edition, 1989.
- [35] J.M. Soler, et al., The SIESTA method for *ab initio* order- *N* materials simulation, J. Phys. Condens. Matter 14 (2002) 2745–2779.
- [36] E.S. Al, et al., Improved grid-based algorithm for bader charge allocation, J. Comput. Chem. 28 (2006) 899–908.
- [37] J.P. Perdew, K. Burke, M. Ernzerhof, Generalized gradient approximation made simple, Phys. Rev. Lett. 77 (1996) 3865–3868.

- [38] A.P. Thompson, et al., Lammps a flexible simulation tool for particle-based materials modeling at the atomic, meso, and continuum scales, Comput. Phys. Commun. 271 (2022) 108171.
- [39] Y. Chen, et al., Recyclable ammonia uptake of a MIL series of metal-organic frameworks with high structural stability, Microporous Mesoporous Mater. 258 (2018) 170–177.
- [40] A. Altmann, L. Toloşi, O. Sander, T. Lengauer, Permutation importance: a corrected feature importance measure, Bioinformatics 26 (2010) 1340–1347.
- [41] T.H. Hung, Q. Lyu, L.C. Lin, D.Y. Kang, Transport-relevant pore limiting diameter for molecular separations in metal-organic framework membranes, J. Phys. Chem. C 125 (2021) 20416–20425.
- [42] P.Z. Moghadam, et al., Structure-mechanical stability relations of metal-organic frameworks via machine learning, Matter 1 (2019) 219–234.
- [43] M.V. Parkes, et al., Molecular dynamics simulation of framework flexibility effects on noble gas diffusion in HKUST-1 and ZIF-8, Microporous Mesoporous Mater. 194 (2014) 190–199.
- [44] T.C. Wang, et al., Ultrahigh surface area zirconium MOFs and insights into the applicability of the BET theory, J. Am. Chem. Soc. 137 (2015) 3585–3591.
- [45] D. Kim, et al., Isoreticular MOFs based on a rhombic dodecahedral MOP as a tertiary building unit, CrystEngComm 16 (2014) 6391–6397.
- [46] J.A. Johnson, et al., A new approach to non-coordinating anions: lewis acid enhancement of porphyrin metal centers in a zwitterionic metal-organic framework, J. Am. Chem. Soc. 138 (2016) 10293–10298.
- [47] D. Sun, Y. Ke, D.J. Collins, G.A. Lorigan, H.C. Zhou, Construction of robust open metal-organic frameworks with chiral channels and permanent porosity, Inorg. Chem. 46 (2007) 2725–2734.
- [48] K. Wang, et al., A series of highly stable mesoporous metalloporphyrin Fe-MOFs, J. Am. Chem. Soc. 136 (2014) 13983–13986.